Journal of Fluids and Structures (2002) **16**(6), 811–840
doi:10.1006/jfls.442 available online at http://www.idealibrary.com on IDEAL®

MODELLING TWO-PHASE FLOW-EXCITED DAMPING AND FLUIDELASTIC INSTABILITY IN TUBE ARRAYS

P. A. Feenstra, D. S. Weaver and R. L. Judd

Department of Mechanical Engineering, McMaster University
Hamilton, Ontario L8S 4L7, Canada

(Received 3 October 2000; and in final form 4 September 2001)

This paper reports the results of an experimental study of the flow-induced vibration of a heat exchanger tube array subjected to two-phase cross-flow of refrigerant 11. The primary concern of the research was to develop a methodology for predicting the critical flow velocities for fluidelastic instability which better characterize the physics of two-phase flows. A new method is proposed for calculating the average fluid density and equivalent flow velocity of the two-phase fluid, using a newly developed void fraction model to account for the difference in velocity between the gas and liquid phases. Additionally, damping measurements in two-phase flow were made and compared with the data of other researchers who used a variety of modelling fluids. The results show that the two-phase damping follows a similar trend with respect to homogeneous void fraction, and when normalized, agree well with the data in the literature. The fluidelastic threshold data of several researchers who used a variety of fluids, is re-examined using the proposed void fraction model, and the results show a remarkable change in trend with flow regime. The data corresponding to the bubbly flow regime shows no significant deviation from the trend established by Connors' theory. However, the data corresponding to the intermittent flow regime show a significant decrease in stability which is nearly independent of the mass-damping parameter. It is believed that the velocity fluctuations that are inherent in the intermittent flow regime are responsible for tripping the instability, causing lower than expected stability of the bundle.

1. INTRODUCTION

Flow-induced vibration is an important concern to designers of thermal hydraulic equipment in which the components are subjected to high-velocity cross-flows of gases or liquids. Nuclear steam generators are an example, in which the U-bend region of the tubes is subjected to a cross-flow of high-velocity steam and water. It is highly undesirable for these tubes to vibrate excessively under normal operating conditions, because tube fatigue or wear and eventual leakage can occur, leading to a costly shutdown for repairs.

It is known that four mechanisms are responsible for the excitation of tube arrays in a cross-flow: turbulence buffeting, Strouhal periodicity, fluidelastic instability, and acoustic resonance. Of these four mechanisms, fluidelastic instability is the most damaging in the short term because it causes the tubes to vibrate excessively, leading to rapid fatigue or wear at the tube supports. This mechanism occurs once the flow rate exceeds a threshold velocity at which the tubes become self-excited and the vibration amplitudes rise rapidly with an increase in flow velocity. Most of the early experimental research in this field relied on sectional scale models of tube arrays subjected to single-phase fluids such as air or water, using relatively inexpensive flow loops and wind tunnels. Complete reviews on the

0889-9746/02/060811 + 30 $35.00/0

topic are provided by Païdoussis (1982) and Weaver & Fitzpatrick (1988). More recently, researchers have expanded the study to two-phase flows, which occur in nuclear steam generators and many other tubular heat exchangers. For an overview of two-phase flow-induced vibration research, see Pettigrew & Taylor (1994).

To study the phenomenon experimentally, the cheapest and simplest approach is to model two-phase flow by mixing air and water at atmospheric pressure. However, air–water flows have a much different density ratio between the phases than steam–water flow and this will affect the difference in flow velocity between the phases. The liquid surface tension, which controls bubble size, is also not accurately modelled in air–water mixtures. For comparison purposes, Table 1 presents some of the liquid and gas phase properties of refrigerant 11 (R-11), refrigerant 22 (R-22), and air–water mixtures at representative laboratory conditions with the actual steam–water mixture properties at typical power plant conditions. This comparison reveals that the refrigerants approximate the density ratio, liquid surface tension and liquid viscosity of steam–water mixtures more accurately than air–water mixtures. There is a clear need for additional research on two-phase flow excitation of heat exchanger tube arrays using experiments which better simulate the actual steam–water flow encountered in service.

Typically, researchers have relied on the Homogeneous Equilibrium Model (HEM) to define the important fluid parameters in two-phase flow such as density, void fraction and velocity. This model treats the two-phase flow as finely mixed and homogeneous in density and temperature, with no difference in velocity between the gas and liquid phases. The HEM has been widely used because it is easy to implement and no reliable alternative was generally available. The main problem with using the HEM is that it assumes a velocity ratio of unity between the gas and liquid phases (i.e., $U_G/U_L = 1$). This assumption is not valid in the case of vertical upward flow, where buoyancy effects due to density differences are significant. As shown in Table 1, the density ratios for the various two-phase fluids used to model steam–water flows are quite different and, thus, so too will be the velocity ratio (slip ratio). Earlier work by the present authors (Feenstra *et al.* 1995) as well as the present study utilized gamma densitometry to measure the actual void fraction in the test-section, and it was found to be much lower than that predicted by the HEM. This led to the development of a new model for predicting the void fraction in upward two-phase flows in horizontal tube bundles. Comparison with other researchers' measurements of void fraction in tube bundles for air–water and R-113, showed remarkably good agreement (Feenstra *et al.* 2000).

This paper presents the results of an experimental study of fluidelastic instability and damping in a parallel triangular tube array subjected to a cross-flow of liquid and two-phase refrigerant 11. The new velocity ratio (slip ratio) model was used to estimate the

TABLE 1

Typical properties of various fluids used to simulate steam–water

Quantity	Steam generator conditions	Air–water	R-11	R-22
Temperature, T (°C)	260	22	40	233
Pressure, P (kPa)	4700	101	175	1000
Liquid density, ρ_L (kg/m^3)	784	998	1440	1197
Vapour density, ρ_G (kg/m^3)	23·7	1·2	9·7	42·3
Density ratio, ρ_L/ρ_G	33	832	148	28
Liquid viscosity, μ_L (μPa s)	103	959	356	139
Surface tension, σ (N m)	0·024	0·073	0·0167	0·0074

actual void fraction and thereby obtain more accurate estimates of the average fluid density and equivalent flow velocity for each experiment. This model was also used to compute these values for the stability data reported in the literature for experiments in air–water, refrigerant 22 and steam–water. Comparisons are then made of the present data with those on a flow regime diagram and on stability graphs.

2. EXPERIMENTAL METHODOLOGY

2.1. Modelling Approach

Typical nuclear steam generators utilize more than 3000 tubes, 13–22 mm in diameter, formed into an inverted U-shape. In the outer U-bend region, the tubes are subject to two-phase cross-flow of steam–water, which is estimated to be 12–20% quality. It is highly impractical and costly to perform flow-induced vibration experiments on a full-scale prototype of such a device, and therefore small-scale sectional modelling is most often adopted. In the present study, the approach is to model a tube span with a cantilevered tube bundle having the same tube layout (i.e., parallel triangular) and the same pitch-to-diameter ratio (i.e., $P/D = 1{\cdot}44$). The first mode natural frequency of the model tubes is 38·8 Hz in air, and about 32 Hz in liquid R-11, which approximates that of the outer most tubes in the U-bend. The tube diameter in the model tube array is 6·35 mm, about one-half the size of the actual steam generator tubes. The length of the tubes is 305 mm, which was determined by the need to match the desired tube frequency within the test-section. The mass per unit length of the model tube is 0·179 kg/m, which was obtained by the judicious selection of thick-walled brass tubes, so that the mass ratio of the tube to the displaced fluid is approximately the same as in the real steam generator. Refrigerant 11 was chosen as the working fluid because it simulates the density ratio, viscosity ratio and surface tension of actual steam–water mixtures better than air–water mixtures and it also allows for localized phase change which air–water mixtures do not permit. While more costly and difficult to use than air–water mixtures, R-11 is a much cheaper modelling fluid than steam–water because it requires 8% of the energy to evaporate the liquid and the operating pressure is much lower, thereby reducing the size and cost of the flow loop. Details of the flow loop and test-section are given in Feenstra *et al*. (1995) and Feenstra (2000).

2.2. Experimental Method

A schematic diagram of the test-section and tube bundle is given in Figure 1. Measurements of tube response were obtained using a fifth row tube, where the flow conditions would be typical of interior tubes in a bundle and not affected by upstream flow conditions. The tube vibration response was measured with a special optical light probe (Judd *et al*. 1992) and processed by a dynamic analyser, which calculates the power spectra for the tube response in the drag and lift directions over a frequency range from 0 to 100 Hz. Thermocouples were used for measuring the fluid temperatures at various locations in the loop and were measured by a multi-point data recorder. Volumetric flow rate into the test-section was measured with an orifice plate. Fluid temperatures as well as heater power were needed for determining the quality of the two-phase flow in the test-section. The amplitude response of the monitored tube in the array was measured at constant mass flux and incrementally increasing void fraction, while the pressure in the loop was kept roughly constant.

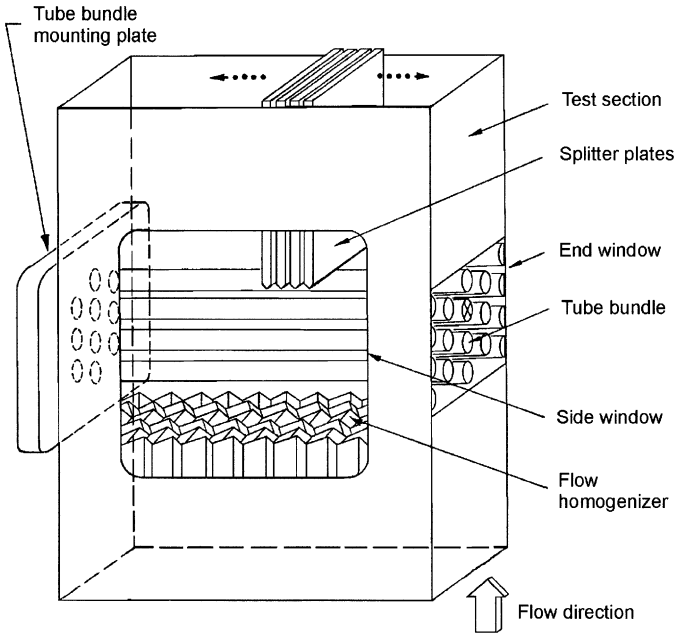

Figure 1. Schematic diagram of test-section with tube bundle installed (monitored tube is marked " × ").

Data acquisition was commenced when steady state conditions were attained, as determined by monitoring the fluid temperatures around the loop. The r.m.s. tip amplitude of the tube and the frequency spectra were determined by a dynamic analyser from at least 100 samples, over a frequency range of 0–100 Hz.

2.3. Determination of Fluid Properties

In the experiments of the present study, two distinct void fraction measurements were made, the HEM void fraction and the RAD void fraction. HEM refers to the Homogeneous Equilibrium Model, and RAD refers to the Radiation Attenuation Detection method. The determination of parameters such as average fluid density and flow velocity are widely different when these two measurement methods are used (Feenstra *et al.* 1995). The subsequent stability analysis of the present data will incorporate both the HEM and RAD void fraction measurements for determining the necessary two-phase fluid properties. In addition, a new model for predicting the actual void fraction in the shell-side flow of horizontal tube arrays has been developed from this work. This model will be used in the fluidelastic stability analysis of other researchers' data to determine the necessary fluid properties. Hence, a comparison can be made of various data sets using the basis of the HEM and the new void fraction model.

2.3.1. *The homogeneous equilibrium model*

A general expression for void fraction, α, is given as

$$\alpha = \left[1 + S\frac{\rho_G}{\rho_L}\left(\frac{1}{x} - 1\right)\right]^{-1}, \tag{1}$$

where ρ_G and ρ_L are the gas and liquid densities, respectively, and S is the velocity ratio (or slip ratio) of the gas and liquid phases (i.e., $S = U_G/U_L$). The quality of the flow, x, is

calculated from an energy balance which requires measurement of the mass flow rate, the temperature of the liquid entering the heater, the heater power, and the fluid temperature in the test-section. The HEM void fraction, α_H, is the simplest of the two-phase fluid models, in which the gas and liquid phases are assumed to be well mixed and velocity ratio, S, is assumed to be unity. The average two-phase fluid density, ρ, is determined by

$$\rho = \alpha\rho_G + (1-\alpha)\rho_L. \tag{2}$$

The HEM fluid density, ρ_H, is determined using equation (2) by substituting α_H in place of α. The HEM pitch flow velocity, V_p, is determined by

$$V_p = G_p/\rho_H. \tag{3}$$

The pitch mass flux, G_p, is determined from flow measurements obtained from an orifice plate by

$$G_p = (\dot{m}/A_u)P/(P-D), \tag{4}$$

where $\dot{m}$ is the measured mass flow rate, A_u is the flow area immediately upstream of the tube array, P is the tube pitch, D is the tube diameter.

2.3.2. *Rad void fraction measurement*

Gamma ray attenuation was used in this study to obtain a void fraction measurement of the two-phase R-11 flow in the test-section. The system consisted of a gamma radiation source, metal shielding, a scintillator and the electronics necessary for signal processing. The basic principle of this device for measuring void fraction [described in detail in Chan & Bannerjee (1981)] is that the gamma flux which penetrates the test-section will be attenuated by different amounts depending upon the average density of the two-phase flow inside. The application of the gamma densitometer in this work was nearly identical to that of Feenstra *et al*. (1995) except that in the present case, a barium-133 source was used. The physical size of the gamma beam was 13 mm high $\times$ 76 m wide. In order to maximize the measurement sensitivity, the gamma beam was passed through the small (open area) gap between the bottom of the tube bundle and the upstream flow homogenizer. It was not desirable to pass the beam through the tube bundle because, given that the height of the beam relative to the tube diameter was not large, any static deflection of the tubes during experiments could throw off the calibration of the device.

The void fraction, α, can be determined by interpolating the average density of the fluid between the benchmark measurements for 100% liquid and gas according to

$$\alpha = \ln(N/N_L)/\ln(N_G/N_L). \tag{5}$$

In this case, N represents the gamma counts obtained during an experimental trial, while N_L and N_G are the reference counts obtained prior to the experiment for 100% liquid and 100% gas, respectively. The individual gas and liquid phase pitch velocities, U_G and U_L, can be calculated by

$$U_G = \frac{xG_p}{\alpha\rho_G}, \quad U_L = \frac{(1-x)G_p}{(1-\alpha)\rho_L}. \tag{6}$$

A better estimate of the average fluid density, ρ, can be computed using the RAD void fraction, α, instead of the HEM void fraction, α_H in equation (2). A realistic measure of flow velocity of vertical upward two-phase flow requires consideration of the difference in phase velocities, as opposed to equation (3) which neglects slip ratio and assumes an average value based upon the mass flux divided by the average fluid density. As will be seen, subsequent analysis of fluidelastic stability data shows that the significant velocity

ratio of the phases in vertical two-phase flow raises serious questions regarding the traditional application of the HEM for calculating average fluid density and flow velocity. In this paper, a new formulation for an equivalent flow velocity for fluidelastic stability analysis, V_{eq}, is introduced according to

$$V_{eq} = \sqrt{[\alpha\rho_G U_G^2 + (1-\alpha)\rho_L U_L^2]/\rho}. \tag{7}$$

This equivalent velocity is based on the assumption that the total kinetic energy of the two phases is a reasonable measure of the fluidelastic excitation energy of the flow. However, it should be noted that equation (7) is based upon intuition only and does not account for intermittency of the flow, void distribution, or details of the local two-phase fluid–structure interaction such as liquid droplet impact. There is a need for future research to establish a more rigorous measure of two-phase flow velocity for the analysis of fluidelastic instability, perhaps through detailed flow velocity measurements.

3. EXPERIMENTAL RESULTS AND DISCUSSION

3.1. Single-Phase Flow Response

3.1.1. *Observed behaviour*

The amplitude response of tube #5 is shown in Figure 2(a) for the fully flexible tube array. The onset of fluidelastic instability occurs at a pitch velocity of about 0·32 m/s (pitch mass flux of about $G_p = 470\,\mathrm{kg/m^2\,s}$), and was accompanied by a slight decrease in vibration frequency. At the stability threshold, the tube motion was a clear whirling pattern with coincidence of the frequencies in the lift and drag directions.

The relatively small peak in the in-line (drag) response at 0·28 m/s pitch velocity corresponds to a Strouhal number of 2·27 based upon the upstream velocity, or 0·70 based upon the pitch velocity (note that, for this tube array, $V_p = 3{\cdot}26V_u$). This is close to the Strouhal number of about 2·0 that is expected for this array type [see Weaver & Fitzpatrick (1988)]. Beyond a pitch velocity of about 0·32 m/s, the overall r.m.s. tube response continues to increase to amplitudes sufficient to cause tube-to-tube clashing and there is little doubt that the tube array has become unstable. While the transition from turbulent to fluidelastic excitation is not as abrupt as typically found for tube bundles in air-flows, the stability threshold (critical velocity) in Figure 2(a) is estimated to be about 0·32 m/s. The undulations in the response in the post-stable region are typical of those expected for the tube arrays in liquid flows; see, for example, Weaver & Koroyannakis (1982).

Experiments were also conducted with all tubes fixed except for the monitored tube, #5. The results for this single flexible tube in a rigid array are shown in Figure 2(b). The stability threshold occurs at a pitch flow velocity of about 0·34 m/s which is slightly higher than for the fully flexible array. The notable difference in behaviour between these two cases is that the single flexible tube responded to flow excitation at essentially a single frequency and the amplitude response did not exhibit the various peaks and troughs characteristic of the response curves for fully flexible arrays in liquid flows. As a result, the stability threshold is more clearly defined in the lower graph. The amplitude response did not reveal any Strouhal peak in the turbulence buffeting region ($V_p < 0{\cdot}34$ m/s), and the vibration mode maintained a nearly circular orbit for the full range of flow velocities tested.

The fact that the stability threshold is roughly the same for the two cases indicates that the dominant fluid forces in single-phase liquid flow are the ones which are proportional to

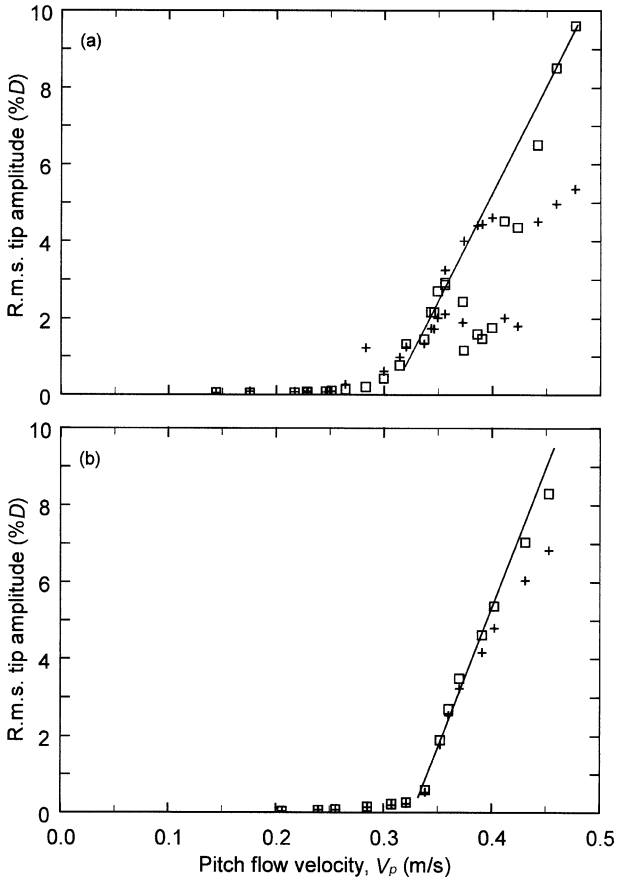

Figure 2. Amplitude response of the tube array subjected to single phase liquid R-11 cross-flow. (a) Fully flexible tube bundle, $V_{p,\mathrm{crit}} = 0{\cdot}32$ m/s. (b) Single flexible tube with other tubes held fixed, $V_{p,\mathrm{crit}} = 0{\cdot}34$ m/s. +, Drag direction; □, lift direction.

tube velocity. When these forces act in phase with tube velocity, the tube is said to be "negatively damped". If the stability threshold had been greatly delayed or absent in the case of the single-flexible-tube bundle, this would indicate that fluidelastic instability is dominated by a displacement mechanism, in which the dominant fluid forces are proportional to tube displacement relative to its nearest neighbours. These findings are in agreement with those of Chen (1983), who concluded that negative damping is the dominant influence in "heavy" fluids, such as water and liquid R-11, while fluid-stiffness-related forces are dominant in "light" fluids, such as air.

3.1.2. *Comparison of fluidelastic results in single-phase flow with other data*

The results for fluidelastic instability in single-phase flow are plotted in Figure 3 on a stability diagram for comparison with other data. This diagram is presented in the form of reduced velocity, V_p/fD, versus mass damping parameter, $m\delta_a/\rho D^2$, and in order to make the comparison consistent, the logarithmic decrement of damping of the tube in quiescent air, δ_a, is utilized. In this study, tube damping in air was determined by analysis of the amplitude decay trace of the monitored tube after plucking, with the other tubes held fixed. The parameters used to determine reduced velocity and the mass damping parameter

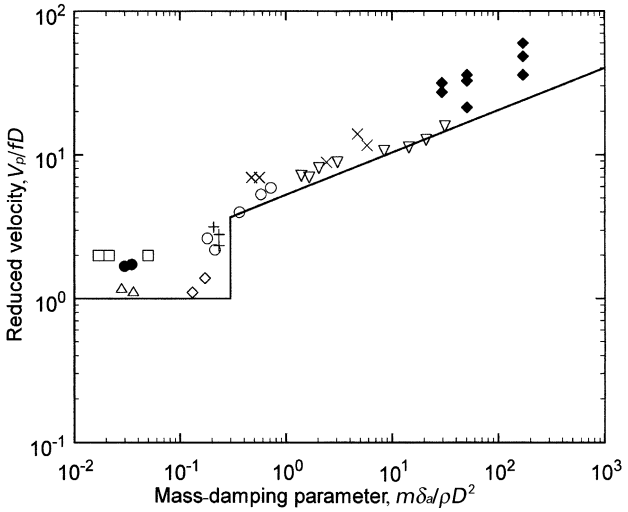

Figure 3. Critical flow velocities for fluidelastic instability of parallel triangular tube arrays in cross-flow: ◆, Hartlen (1974) in air; □, Weaver & Yeung (1984) in water; △, Weaver & Koroyannakis (1982) in water; ◇, Scott & Weaver (1986) in water; ○, Heilker & Vincent (1981) in air–water; ▽, Weaver & Grover (1978) in air; +, Gorman (1976) in water; ×, Pettigrew *et al.* (1978) in air–water; ●, present study in liquid R-11; ———, Weaver & Fitzpatrick (1988).

for the monitored tube at the stability threshold in single-phase flow are given as follows: for the fully flexible array, $\delta_a = 2\pi\zeta_a = 0{\cdot}0069$, $V_p = 0{\cdot}32$ m/s, $f = 29{\cdot}3$ Hz, $f_a = 38{\cdot}0$ Hz, $D = 0{\cdot}00635$ m, $m_t = 0{\cdot}174$ kg/m, $\rho = 1480$ kg/m^3, so that the critical reduced velocity is 1·72 and the mass-damping parameter is 0·035. For the single flexible tube in the rigid array, $V_p = 0{\cdot}$ m/s, $f = 31{\cdot}8$ Hz and $m = 0{\cdot}256$ kg/m, so that the reduced velocity is 1·68 and the mass-damping parameter is 0·030. These two single-phase data points are plotted in Figure 3 and they are in reasonable agreement with previous empirical results obtained from other experiments in single-phase flow of air and/or water.

3.2. Two-Phase Flow Response

Figure 4 presents some typical amplitude response curves of the fully flexible tube array that clearly illustrates the phenomenon of fluidelastic instability. Below the critical flow velocity, the monitored tube responds to increasing flow by a gradual increase in vibration amplitude, but beyond the threshold velocity, the vibration amplitude suddenly increases at a much greater slope, especially in the lift direction. In each graph, the pitch mass flux through the test-section was held constant while the void fraction was increased by increasing the heating of the R-11 flow. Hence the HEM pitch flow velocity increases by virtue of a reduction in the average density of the fluid from one trial to the next. The stability threshold in the fully flexible array is fairly well defined in all cases, which was the main reason for adopting the present experimental method.

A comparison between the response of the tube in the fully flexible array and the single flexible tube in the rigid array is shown in Figure 5 for two pitch mass fluxes. For the single flexible tube case, the fluidelastic threshold is surprisingly absent at the conditions for which it occurred in the flexible array. The stability threshold for these cases might have been reached at a higher void fraction but this was not obtainable because of performance limitations of the flow loop. That the stability threshold is delayed or eliminated for the

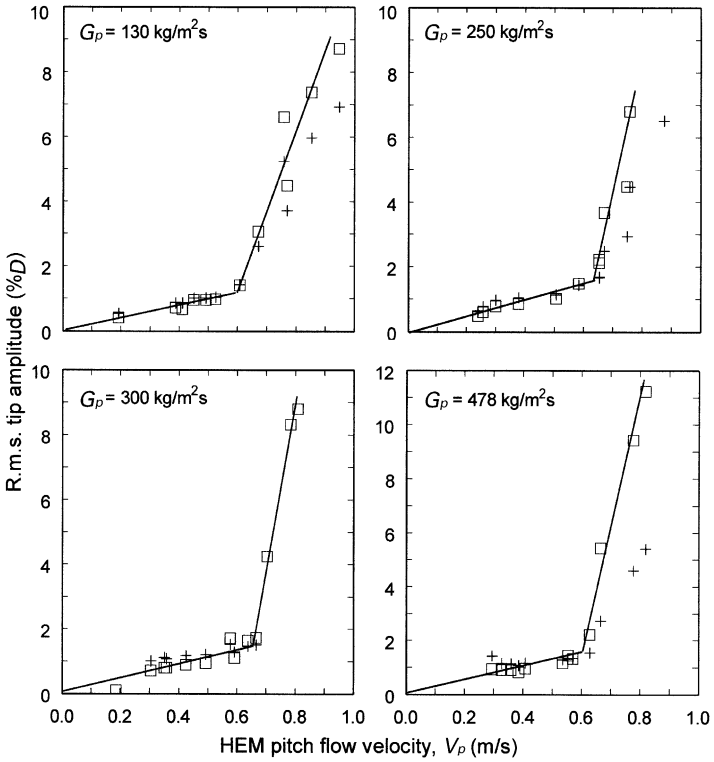

Figure 4. Amplitude response of the tube array subjected to two-phase R-11 cross-flows of various mass fluxes. +, Drag direction; □, lift direction.

single-flexible-tube bundle case suggests that the mechanism for fluidelastic instability in two-phase flow may be dominated by a fluid-stiffness mechanism (i.e., tube coupling) rather than a fluid-damping mechanism, contrary to the case for single-phase liquid flow. However, it should be noted that Lever & Weaver (1986) found the same stability threshold for both cases in air-flow for this array. In any event, it is clear that the presence of two-phase flow appreciably influences the mechanism of self-excitation for a single flexible tube in a rigid bundle.

Interestingly, for equivalent flow conditions which lie below the fluidelastic threshold, in the turbulence buffeting region, the vibration amplitudes are about the same for the flexible and rigid tube arrays. Similar findings were reported by Pettigrew *et al.* (1989*b*) in two-phase air–water flow and by Pettigrew *et al.* (1995) in two-phase R-22 flow. This demonstrates the equivalency of the single-flexible-tube and fully-flexible-tube arrays for the determination of turbulence buffeting forces and fluid damping.

Representative frequency spectra for two experiments are given in Figure 6 for the lift direction, where the first four graphs, (a)–(d), correspond to the fully flexible tube array while the last four, (e)–(h), correspond to the single flexible tube in the rigid array. Note that the ranges for the vertical scale (r.m.s. tip amplitude) are not all the same. In the case of the fully flexible array for conditions below the stability threshold, it is apparent that there are two distinct frequency peaks of vibration. The lower of these two frequency peaks ranges from roughly 32 Hz at low void fraction to 37 Hz at the highest void fraction levels. This peak steadily shifts towards a higher frequency as the void fraction is increased, until it merges with the other peak. The second peak occurs at roughly 36 Hz at

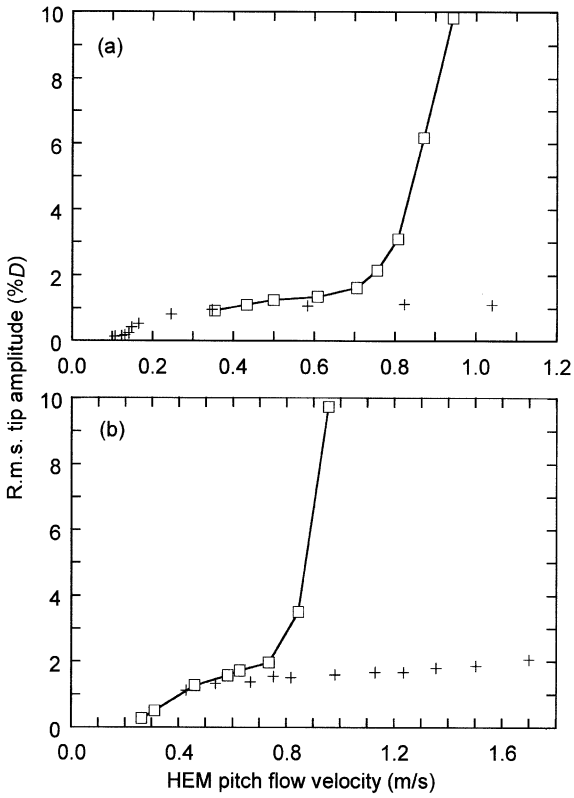

Figure 5. Typical amplitude response curves for two-phase R-11 cross-flow. Comparison of response amplitudes for the fully flexible and single flexible tube arrays for a pitch mass flux of (a) 150 kg/m^2 s and (b) 350 kg/m^2 s.

low void fraction, and increases to about 37 Hz when the fluidelastic stability threshold is reached. This behaviour can be explained by the significant influence of relative tube motion on fluid added mass. The onset of fluidelastic instability in the flexible array occurred roughly at the same time as these two frequency peaks merged. For the case of the single flexible tube array, the two-peak phenomenon is virtually absent, and the spectra more resemble that of a single-degree-of-freedom system subjected to random excitation. For this reason, damping measurements were obtained using this tube array.

3.3. Flow Regime

A discussion of flow regime is necessary to set the stage for the subsequent comparison of fluidelastic data. A vertical flow of two-phase gas and liquid will assume various flow patterns and distribution of phases depending mostly upon the flow quality, the density ratio of the two-phases and the total mass flux. The map used to predict the various flow patterns in this study is illustrated in Figure 7. The abscissa and ordinate are in terms of the superficial gas and liquid phase velocities (U_{Gs} and U_{Ls}), respectively, which are defined as

$$U_{Ls} = (1 - x)G_p/\rho_L, \quad U_{Gs} = xG_p/\rho_G. \tag{8}$$

The solid lines in Figure 7 represent transition boundaries determined by Ulbrich & Mewes (1994), who performed an exhaustive analysis of available flow regime data in

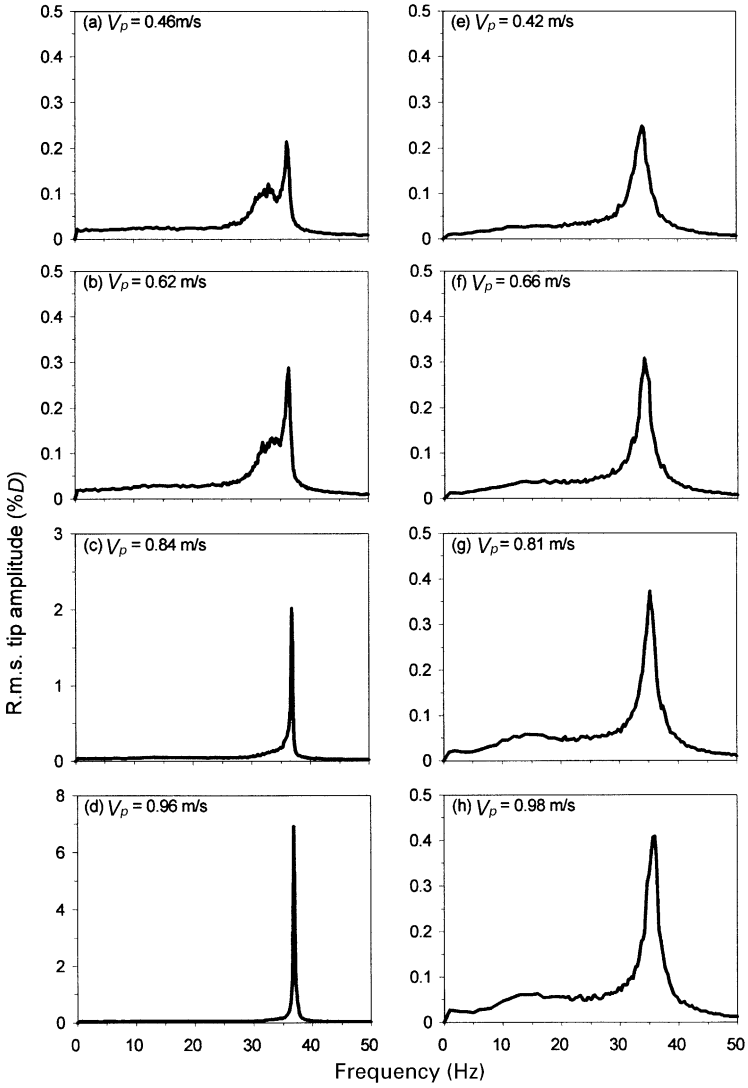

Figure 6. Frequency spectra of the monitored tube in the lift direction for a pitch mass flux of 350 $kg/m^2 s$. Graphs (a)–(d) correspond to the fully flexible tube bundle, and graphs (e)–(h) to the single flexible tube bundle.

vertical two-phase cross-flow through horizontal tube bundles. They found that the flow patterns observed and those plotted on the traditionally used maps of Taitel *et al.* (1980) and Grant & Murray (1972), showed only a 46 and 50% rate of agreement, respectively. Consequently, they developed a flow pattern map more appropriate for cross-flow in a tube bundle, with a new set of boundaries which had an 86% rate of agreement with data from the literature. The flow regime boundaries must be considered as approximate. Figure 7 gives this flow regime map showing the stability threshold data of the present study together with data from the literature (Pettigrew *et al.* 1989*b*, 1995; Axisa *et al.* 1985). Most of these data sets appear to cross over from the bubbly to the intermittent

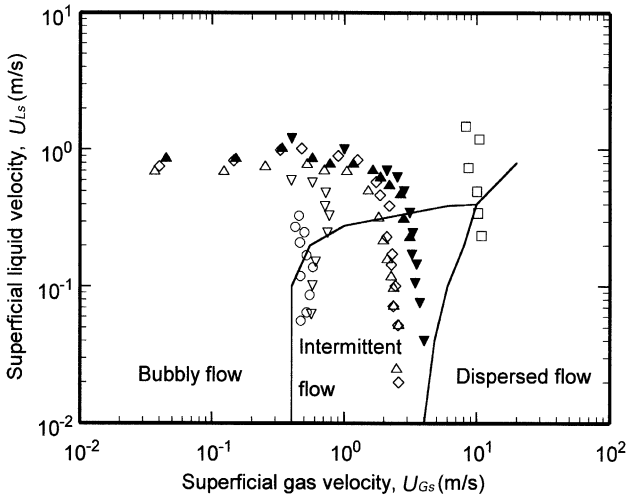

Figure 7. Flow regime map developed by Ulbrich & Mewes (1994). Fluidelastic threshold data of: ○, present study in R-11; □, Axisa *et al.* (1985) in steam–water; ▲,△,▼,◇, Pettigrew *et al.* (1989*b*) in air–water; ▽, Pettigrew *et al.* (1995) in R-22.

flow regimes. This is of particular interest, because the subsequent analysis suggests that a different fluidelastic behaviour exists between these two flow regimes.

3.4. Void Fraction Determination

An empirical model for predicting the void fraction in upward two-phase flows through horizontal tube bundles has been developed by the present authors from the work of this and previous studies. This model was tested against other researchers' measurements of void fraction in tube bundles for air–water and R-113, and remarkably good agreement was observed. Figure 8 shows a sample set of results from the paper by Feenstra *et al.* (2000), where this newly developed void fraction model was first introduced. This figure shows the comparison of RAD void fraction measurements of the present study with various void fraction models, including the HEM, the drift flux model developed by Zuber & Findlay (1965), the empirical models developed by Dowlati *et al.* (1992) and Schrage *et al.* (1988), and the new void fraction model. Two points are illustrated by this graph: the HEM greatly overpredicts the actual gamma densitometer void fraction measurements, and the prediction of the new void fraction model is superior to that of the other models. Feenstra *et al.* (2000) also showed that their new model agreed well with data in the literature for air–water and R-113 over a wide range of mass flux and array geometries. The new void fraction model, which predicts the velocity ratio of the phases, is given by

$$S = 1 + 25{\cdot}7(\mathrm{Ri} \times \mathrm{Cap})^{0{\cdot}5}(P/D)^{-1}, \tag{9}$$

where the velocity ratio, S, is used in conjunction with equation (1) to determine the actual void fraction, α. The Richardson number, Ri, is calculated by

$$\mathrm{Ri} = \Delta\rho^2 ga/G_p^2, \tag{10}$$

where a is the gap between the tubes, $\Delta\rho$ is the density difference between the phases (i.e., $\Delta\rho = \rho_L - \rho_G$) and g is the gravitational acceleration. The Capillary number, Cap,

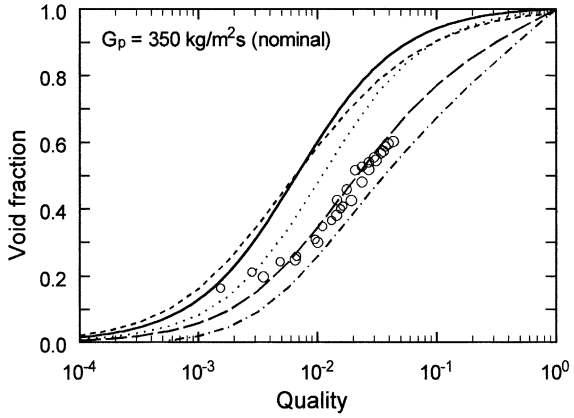

Figure 8. Comparison of void fraction models with measurements of the present study in R-11 cross flows for $G_p = 350\,\mathrm{kg/m^2\,s}$ nominal. (———, HEM; - - - Dowlati *et al.* (1992); ···, drift flux; –·–·–, Schrage *et al.* (1988); — — —, new void fraction model. ○, Experimental RAD void fraction measurements.

is calculated by

$$\mathrm{Cap} = \mu_L U_G/\sigma, \tag{11}$$

where μ_L is the liquid-phase absolute viscosity, σ is the liquid surface tension and U_G is the gas-phase velocity determined from equation (6). This void fraction model is utilized in this paper to obtain more accurate estimates of average fluid density and flow velocity of other researchers' data sets for subsequent stability analysis.

3.5. Damping and Hydrodynamic Mass

The damping and hydrodynamic mass measurements in two-phase flows reported here were obtained from the single flexible tube in an otherwise rigid array. Damping was measured using the half-power bandwidth method, applied to the frequency response function that was obtained from the output of the light probe. Previous research by Weaver & Koroyannakis (1982) and by Harris *et al.* (1985) showed that measuring damping of a tube with the others held fixed prevented amplitude modulation and energy transfer to and from neighbouring tubes through fluid coupling.

The use of the half-power bandwidth method requires that the flow excitation be time invariant, broadband random in the vicinity of the tube natural frequency and that the vibratory system must be a linear, time invariant and of a single degree of freedom. However, for closely spaced tube bundles in a dense medium, hydrodynamic coupling violates the assumption of a time-invariant and single-degree-of-freedom system, because each structural mode exhibits a number of natural frequencies corresponding to varying added mass associated with different relative modes between adjacent tubes. This generally results in a broadening of the measured frequency spectra of the monitored tube when subjected to random broadband excitation. Application of the half-power bandwidth method to such a broadened spectra would result in unrealistically high damping measurements. This was observed by Pettigrew *et al.* (1989*a*), who also reported damping measurements with a single flexible tube bundle in a two-phase air–water cross-flow. Thus, using a single flexible tube in a rigid array has been shown to give reliable damping data and is commonly used for tube bundles in liquid or two-phase flows where fluid coupling is significant.

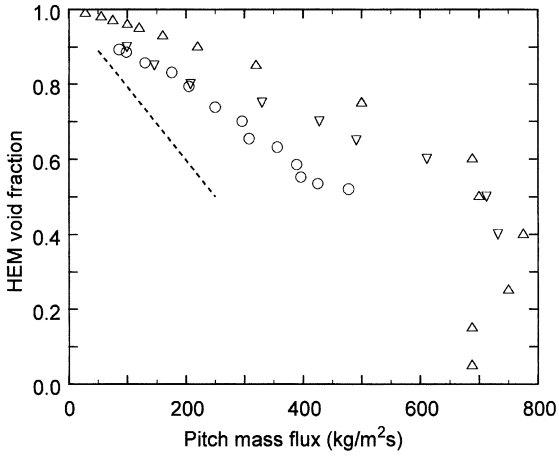

Figure 9. Summary of conditions corresponding to the fluidelastic stability threshold for fully flexible, parallel triangular arrays subjected to two-phase cross-flow; ○, present study in R-11; △, Pettigrew *et al.* (1989*b*) in air–water; □, Pettigrew *et al.* (1995) in R-22. - - -, Required experimental conditions to obtain damping measurements at half the critical mass flux.

To be consistent with the method of Pettigrew *et al.* (1989*a*, *b*, 1995) for reducing the fluidelastic data, special care was taken to obtain damping values at half the critical mass flux. The fluidelastic stability threshold data points from the present study in Figure 9 illustrate that a nearly linear relationship exists between the HEM void fraction and pitch mass flux for conditions at the stability threshold. The data of Pettigrew *et al.* (1989*b*, 1995) are plotted as well, to illustrate that a similar behaviour was observed in air–water and in R-22 for a mass flux less than about 650 $kg/m^2 s$. The dotted line represents the conditions at half the mass flux for instability for the present study, and was used in subsequent experiments as a target for obtaining the required conditions for damping and hydrodynamic mass measurements. This line extends only over a limited range of HEM void fraction from about 54 to 89%. Conditions above 89% HEM void fraction are out of range because it is not practical to operate the flow loop at a pitch mass flux less than about 50 $kg/m^2 s$. HEM void fraction below 54% is out of range because the required threshold flow velocity requires a pitch mass flux in excess of 500 $kg/m^2 s$, which is the present maximum capacity of the flow loop.

3.5.1. *Damping in two-phase flow*

The damping data for this study are presented in Figure 10(a) as a function of HEM void fraction, obtained from a least-squares regression fit to the frequency spectra of tube #5, which was averaged over 600 s of data with a frequency resolution of 0·125 Hz. It is clear that the measured damping is consistently lower in the lift direction, which is also the direction that the tube becomes fluidelastically unstable.

In Figure 10(b), the average damping data of the present study (average of the lift and drag direction) are compared with damping data of Pettigrew *et al.* (1989*a*, 1995) for air–water and R-22 and Axisa *et al.* (1985) for steam–water. This figure illustrates that the measured damping ratios, ζ, of the present study are roughly the same as the air–water and steam–water data above 70% homogeneous void fraction, but somewhat lower at void fractions below 70%. Table 2 contains the essential damping data for the present study as well as for the other studies used for comparison in this paper.

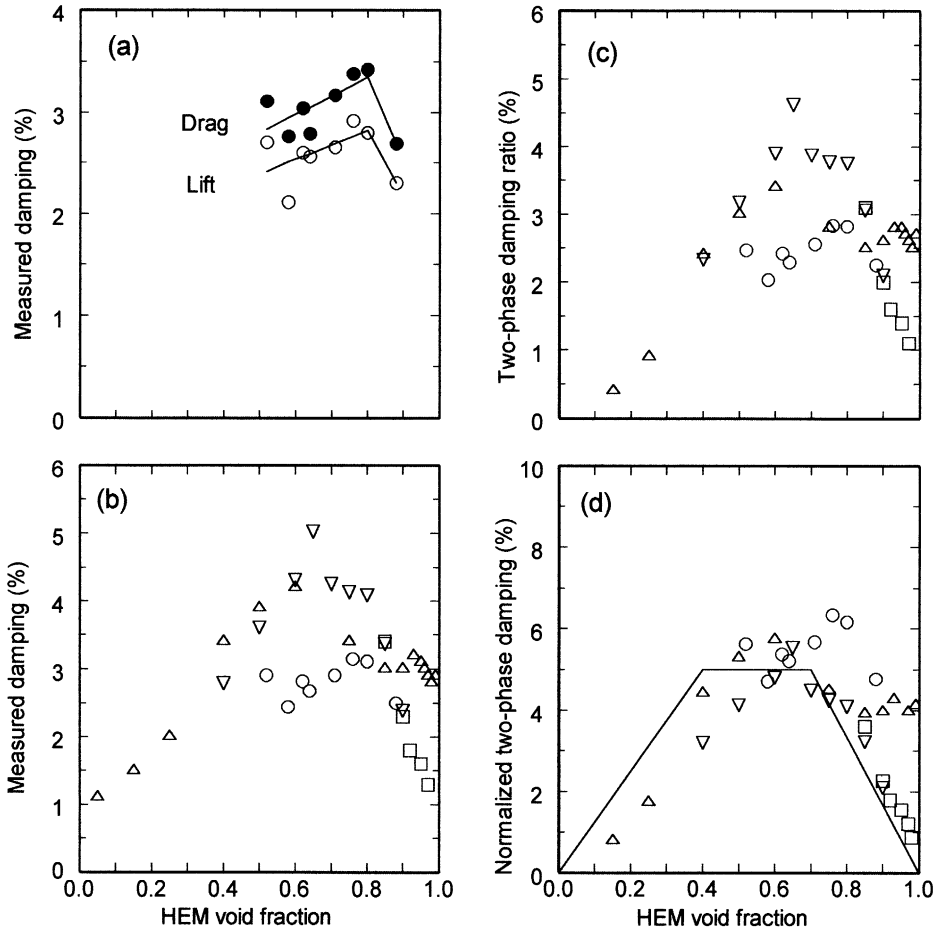

Figure 10. Summary of damping measurements for a single flexible tube in parallel triangular arrays, subjected to two-phase cross-flow. (a) Present study in R-11: ○, lift direction; ●, drag direction. (b) Measured damping comparison, (c) two-phase damping comparison and (d) normalized two-phase damping comparison: ○, present study in R-11; △, Pettigrew *et al.* (1989*b*) in air–water; ▽, Pettigrew *et al.* (1995) in R-22; □, Axisa *et al.* (1985) in steam–water.

In Figure 10(c), the average two-phase damping data of the present study are compared with those of the other studies. The two-phase component of tube damping, ζ_{TP}, is found when the structural, ζ_S, and viscous components, ζ_V, are subtracted from the measured damping, (i.e., $\zeta_{TP} = \zeta - \zeta_S - \zeta_V$). The structural damping component of the other cases was 0·2% or less, so that it represents a nearly negligible component of the overall damping. The viscous component of damping is given by

$$\zeta_V = \frac{\pi}{8}\left(\frac{\rho_H D^2}{m}\right)\left(\frac{2v_{TP}}{\pi f D^2}\right)^{0.5}\frac{[1+(D/D_e)^3]}{[1-(D/D_e)^2]^2}, \tag{12}$$

which varies inversely with void fraction (Pettigrew *et al.* 1986). It can been seen in Table 2 that this component diminishes at high void fraction. The two-phase viscosity, v_{TP}, follows the method of McAdams *et al.* (1942),

$$v_{TP} = \frac{v_L}{1+\alpha_H(v_L/v_G - 1)}. \tag{13}$$

TABLE 2

Summary of damping data analysis for parallel triangular arrays in two-phase cross-flow

Test no.	α_H (%)	f (Hz)	ρ (kg/m^3)	m (kg/m)	v_{TP} (μN/m)	Damping ratio (%)				
						ζ	ζ_s	ζ_v	ζ_{TP}	$(\zeta_{TP})_D$
Present study: R-11, 36°C, $P/D = 1{\cdot}44$, $D = 0{\cdot}00635$ m, $D/D_e = 0{\cdot}413$										
$v_L = 2{\cdot}57 \times 10^{-7}$ m^2/s, $v_G = 1{\cdot}32 \times 10^{-6}$ m^2/s, $\rho_L = 1450$ kg/m^3										
A	52	35·7	699	0·203	0·44	2·91	0·11	0·33	2·47	5·6
B	58	35·8	607	0·202	0·48	2·44	0·11	0·30	2·03	4·7
C	62	35·4	556	0·208	0·51	2·82	0·11	0·29	2·42	5·4
D	64	36·1	531	0·199	0·53	2·68	0·11	0·27	2·29	5·2
E	71	35·7	427	0·204	0·60	2·91	0·11	0·24	2·56	5·7
F	76	35·5	355	0·207	0·66	3·15	0·11	0·21	2·83	6·3
G	80	35·1	295	0·211	0·72	3·11	0·11	0·18	2·82	6·2
H	88	36·7	183	0·192	0·88	2·49	0·11	0·13	2·25	4·8
Pettigrew *et al.* (1989*a*): air–water, 22°C, $P/D = 1{\cdot}47$, $D = 0{\cdot}013$ m, $D/D_e = 0{\cdot}403$										
$v_L = 1{\cdot}0 \times 10^{-6}$ m^2/s, $v_G = 1{\cdot}47 \times 10^{-5}$ m^2/s, $\rho_L = 998$ kg/m^3										
R-2	15	26·8	850	0·50	1·2	1·5	0·2	0·93	0·4	0·8
R-3	25	27·0	750	0·49	1·3	2·0	0·2	0·87	0·9	1·7
R-4	40	27·7	600	0·47	1·6	3·4	0·2	0·76	2·4	4·4
R-5	50	28·3	501	0·45	1·9	3·9	0·2	0·68	3·0	5·3
R-6	60	28·9	401	0·43	2·3	4·2	0·2	0·59	3·4	5·7
R-7	75	29·5	251	0·41	3·3	3·4	0·2	0·44	2·8	4·5
R-9	85	30·0	151	0·40	4·8	3·0	0·2	0·32	2·5	3·9
R-11	90	30·2	101	0·39	6·3	3·0	0·2	0·24	2·6	4·0
R-15	95	30·4	51	0·39	8·8	3·1	0·2	0·14	2·8	4·3
R-19	97	30·4	31	0·39	11·0	2·9	0·2	0·10	2·6	4·0
R-23	99	30·5	11	0·39	13·0	2·9	0·2	0·04	2·7	4·1

Axisa *et al.* (1985): steam–water, 210°C, $P/D = 1{\cdot}44$, $D = 0{\cdot}0191\,\mathrm{m}$, $D/D_e = 0{\cdot}413$
$v_L = 1{\cdot}5 \times 10^{-7}\,\mathrm{m^2/s}$, $v_G = 1{\cdot}66 \times 10^{-6}\,\mathrm{m^2/s}$, $\rho_L = 852\,\mathrm{kg/m^3}$

A	84·7	69·0	145	0·56	0·59	3·4	0·2	0·07	3·1	3·6
B	89·7	69·8	101	0·55	0·74	2·3	0·2	0·05	2·0	2·3
C	92·1	70·0	80	0·54	0·85	1·8	0·2	0·05	1·6	1·8
D	95·3	72·0	51	0·53	1·0	1·6	0·2	0·03	1·4	1·6
E	96·7	71·0	39	0·53	1·2	1·3	0·2	0·03	1·1	1·2
F	97·8	71·8	29	0·53	1·3	1·0	0·2	0·02	0·8	0·9

Pettigrew *et al.* (1995): R-22, 23\kern-1pt ·\kern-1pt 3°C, $P/D = 1{\cdot}5$, $D = 0{\cdot}0127\,\mathrm{m}$, $D/D_e = 0{\cdot}389$
$v_L = 1{\cdot}36 \times 10^{-7}\,\mathrm{m^2/s}$, $v_G = 3{\cdot}02 \times 10^{-7}\,\mathrm{m^2/s}$, $\rho_L = 1197\,\mathrm{kg/m^3}$

A	40	23·9	737	0·39	3·31	2·8	0·2	0·26	2·3	3·2
B	50	24·6	621	0·37	3·73	3·6	0·2	0·24	3·2	4·1
C	60	25·0	505	0·35	4·34	4·3	0·2	0·21	3·9	4·8
D	65	25·3	448	0·34	4·76	5·0	0·2	0·20	4·6	5·5
E	70	25·8	390	0·33	5·31	4·3	0·2	0·18	3·9	4·5
F	75	26·0	332	0·32	6·06	4·1	0·2	0·16	3·8	4·3
G	80	26·3	274	0·31	7·11	4·1	0·2	0·14	3·8	4·1
H	85	26·9	216	0·30	8·73	3·4	0·2	0·11	3·1	3·2
I	90	27·5	158	0·29	11·5	2·4	0·2	0·09	2·1	2·2

The normalized two-phase component of damping ratio, $(\zeta_{TP})_D$, is plotted in Figure 10(d) along with the other data. Though it is not yet known which parameters are valid for normalizing the two-phase damping data for different fluids, the present study follows a method proposed by Pettigrew & Taylor (1994)

$$(\zeta_{TP})_D = \zeta_{TP}\left[\frac{m}{\rho_L D^2}\right]\left[\frac{(1-(D/D_e)^2)^2}{1+(D/D_e)^3}\right], \tag{14}$$

where ζ_{TP} is the two-phase damping component and the other two parameters in the square brackets are the mass ratio, $m/\rho_L D^2$, and the inverse confinement function. The confinement term, D/D_e, follows the work of Rogers *et al.* (1984) and is given by

$$D/D_e = \left[\left(0{\cdot}96 + 0{\cdot}5\frac{P}{D}\right)\frac{P}{D}\right]^{-1}. \tag{15}$$

Interestingly, the comparison reveals that the present normalized damping data agree reasonably well with the air–water data of Pettigrew *et al.* (1989*a*) and the R-22 data of Pettigrew *et al.* (1995). The explanation for the relative upward shift in magnitude between the R-11 data and the air–water data from (c) to (d) in Figure 10 can be found by examining the terms used to normalize the data. In both the R-11 and air–water results, the confinement functions were roughly equal at 1·55 and 1·52, respectively, because this function is fixed by the array type and the P/D ratio and was about the same for all of the comparison data. However, the mass ratio in liquid, $m/\rho_L D^2$, is significantly lower for the R-11 data than for the air–water and R-22 data, which caused the upward shift in the magnitude of the R-11 data when it was normalized using equation (14).

It is noteworthy that the damping data of the present study achieved satisfactory agreement with the air–water and R-22 data without any correction for surface tension effects. However, initial experiments by Pettigrew & Knowles (1997) in air–water showed a roughly linear correlation between damping and surface tension of the liquid phase for lower tube frequencies (i.e., 28 Hz and lower). They proposed that an additional surface tension term might be appropriate in equation (14) such as

$$\text{Surface tension term} = \left[\frac{\sigma_T}{\sigma_{\text{water, 20°C}}}\right]^{-1}, \tag{16}$$

where $\sigma_{\text{water, 20°C}}$ represents the surface tension of ambient pure water. However, if equation (16) were included as a normalizing parameter in equation (17), then the R-11 damping results in Figure 10(d) would increase by a factor of about 4 (verified easily by comparing the surface tension data in Table 1), which would set them far apart from the other data. This suggests that the effect of surface tension is not as strong as first believed, but there are a number of issues which must be resolved before a reliable design factor can be devised to account for it. Firstly, it is well known that a small amount of contaminant in the liquid can significantly decrease the surface tension from the published value, so that a reliable measurement method of the actual liquid surface tension is required. Secondly, the initial work by Pettigrew & Knowles (1997) did not extend beyond 25% void fraction, and their results for tube frequencies of 28 Hz tended towards a decreasing dependence on surface tension as the void fraction was increased from 5 to 15 to 25%. Hence the effect of surface tension is excluded from this analysis until more comprehensive data become available and a more reliable surface tension scaling parameter is determined.

3.5.2. *Hydrodynamic mass in two-phase flow*

Figure 11(a) illustrates the hydrodynamic mass ratio as a function of HEM void fraction. Hydrodynamic mass is the fluid added mass (or virtual mass) which appears to vibrate with the tube. Hydrodynamic mass ratio, m_R, is the added fluid mass divided by the added mass of the liquid phase determined according to

$$m_R = \frac{(f_a/f)^2 - 1}{(f_a/f_L)^2 - 1}, \tag{17}$$

where f, f_a and f_L are the tube vibration frequencies in two-phase flow, in still air and in still liquid, respectively. The measurements were obtained from tube #5 in the single flexible tube array. In these graphs, the data points correspond to measured hydrodynamic mass ratio for various mass fluxes. The solid lines in Figure 11(a,b) represent the predicted hydrodynamic mass ratio according to

$$m_{R,\,\mathrm{pred}} = \frac{\rho_{\mathrm{HEM}}}{\rho_L} \quad \text{or} \quad \frac{\rho_{\mathrm{RAD}}}{\rho_L}. \tag{18}$$

The data in the upper graph, Figure 11(a), shows generally a higher hydrodynamic mass ratio than predicted using the HEM void fraction. This is expected, since it was earlier

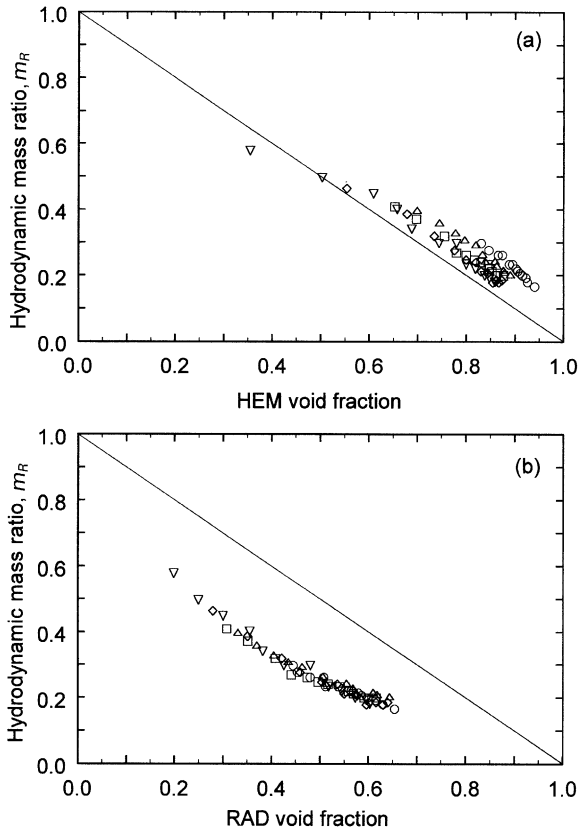

Figure 11. Measured data for hydrodynamic mass ratio, m_R, for the single flexible tube bundle subjected to two-phase R-11 cross-flow. Comparison of measurement and theory using (a) HEM void fraction, and (b) RAD void fraction. Data correspond to a pitch mass flux (G_p) of: ○, 150; △, 200; □, 250; ◇, 300; ▽, 350 kg/m^2 s. ———, Predicted mass ratio.

demonstrated that the HEM generally overpredicts the relative amount of vapour phase in the flow and thus it is expected to predict a lower added mass. However, in Figure 11(b), the data shows a lower hydrodynamic mass ratio than predicted using the RAD void fraction. This is not expected, however, because the RAD void fraction is a better measure of the actual void fraction in the flow than the HEM. It appears as if the tube vibrates in a "lighter" fluid than indicated by the RAD void fraction.

3.6. Fluidelastic Instability in Two-Phase Flow

3.6.1. *Comparison of fluidelastic results with data from the literature*

Four sets of fluidelastic instability results are plotted in Figure 12(a) in terms of critical reduced velocity versus mass damping parameter: the present data in R-11, $P/D = 1{\cdot}44$; Pettigrew *et al.* (1989*b*) in air–water, $P/D = 1{\cdot}47$; Axisa *et al.* (1985) in steam–water, $P/D = 1{\cdot}44$; and Pettigrew *et al.* (1995) in R-22, $P/D = 1{\cdot}5$. In this figure, the HEM is used to calculate the pitch flow velocity, V_p, and average fluid density, ρ_H, which is the traditional approach. Mass-damping parameter is given by $m\delta/\rho_H D^2$, where δ is the in-flow logarithmic decrement damping value, and ρ_H is the average density of the two-phase

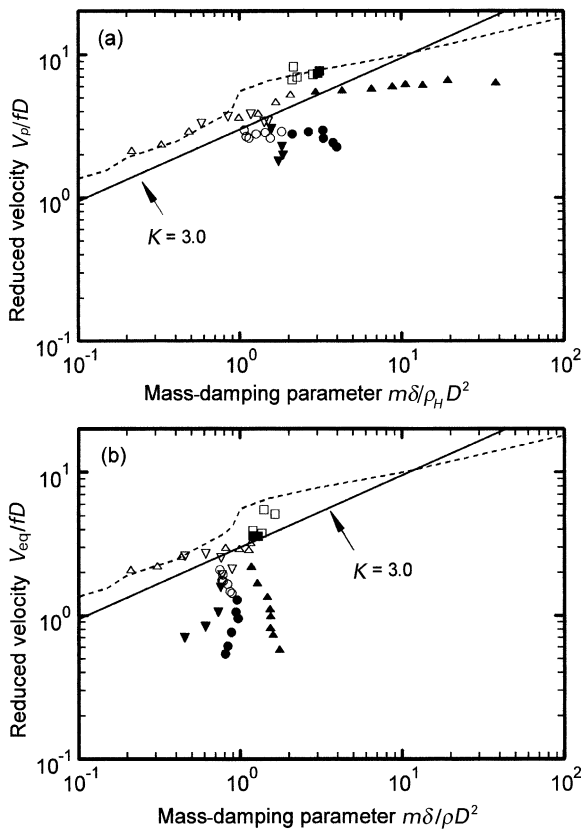

Figure 12. Critical flow velocities for fluidelastic instability of parallel triangular tube arrays in two-phase cross-flow. Data analysis by (a) HEM model, and (b) void fraction model: ○,●, present study in R-11; △,▲, Pettigrew *et al.* (1989*b*) in air–water; ▽,▼, Pettigrew *et al.* (1995) in R-22; □,■, Axisa *et al.* (1985) in steam–water; ———, Connors' theory; - - - -, prediction of Li & Weaver (1997). ○,△,▽,□, Bubbly flow; ●,▲,▼, intermittent flow; ■ dispersed flow.

flow, which is calculated using equation (2). The mass per unit length, m, is the mass of the tube per unit length including fluid hydrodynamic mass, which is determined by

$$m = m_t(f_a/f)^2, \tag{19}$$

where m_t is the mass per unit length of the tube in air while f_a and f are the tube vibration frequencies in-air and in-flow respectively. The in-flow damping, δ, was used to plot this data, where for all results except for Axisa *et al.* (1985), the damping value was obtained from half-power bandwidth measurements of a single flexible tube in a rigid array at half the mass flux for fluidelastic instability. This simply follows the practice developed by Pettigrew *et al.* (1989*a*). Axisa *et al.* measured damping in the fully flexible bundle, but the void fraction range of their data was high, so that fluid coupling was likely less of a problem.

The design criterion of Pettigrew & Taylor (1994) for the determination of critical flow velocity is indicated by the solid line on Figure 12 for P/D ratios of between 1·4 and 1·5 in continuous flow regimes (i.e., bubbly). This follows from Connors' relationship

$$V_p/fD = K\sqrt{m\delta/\rho_H D^2}, \tag{20}$$

where $\delta \approx 2\pi\zeta$. This relationship predicts that the critical reduced velocity should vary with mass-damping parameter to the one-half power, and the so-called "Connors constant" should be $K = 3{\cdot}0$. Also plotted on this figure is the theoretical stability prediction of Li & Weaver (1997) for parallel triangular arrays of $P/D = 1{\cdot}5$, which was developed for single-phase flow. The data points in this figure have been distinguished between the different predicted flow regimes, where the open symbols correspond to bubbly flow and the solid symbols represent intermittent flow, except for Axisa *et al.* where the solid symbols represent the dispersed (annular) flow regime. Of particular note in this figure is that the air–water data show a distinct change in slope while the R-22 and some of the R-11 data show a decrease in stability. All of these effects coincide with a predicted flow regime change from bubbly to intermittent flow.

The present data corresponding to the bubbly flow regime show a lower stability threshold than most of the other data of the bubbly flow type, where an appropriate lower bound for Connors' constant would be about $K = 2{\cdot}0$. A possible reason for the difference could be the effect of using different modelling fluids, since the majority of the earlier data which were obtained in air–water. R-11 is a single component fluid while air–water is a two-component fluid which cannot simulate the local formation or collapse of vapour on the tube surfaces. This could be a factor affecting the tube forces in the steam generator tube bundle which is subjected to steam–water. However, the steam–water results of Axisa *et al.* (1985) show a higher stability than the air–water results, corresponding to a lower bound Connors' constant of $K = 4{\cdot}2$. Thus, the effect of two component versus single component modelling fluids remains unclear based upon this simple comparison. Another difference between the present results and other data is the physical scale of the model. This study used 6·35 mm ($1/4''$) diameter tubes while the other studies used full-scale tube diameters of 12·7 mm ($\frac{1}{2}''$) or greater. It is generally accepted that, using dimensionless parameters to compare model and prototype behaviour, correctly handles scale effects, so the physical dimensions of laboratory models and prototypical structures vary substantially. However, two-phase flows are a special case, because of the presence of vapour bubbles or liquid droplets. Clearly, the size of these bubbles or droplets compared to the tube dimensions could play an important role in determining the magnitude of these fluid forces. Additionally, void coalescence or liquid slugging can occur, leading to intermittent flows. These effects are determined, in part, by

TABLE 3

Summary of fluidelastic instability data for parallel triangular arrays

Test no.	G_p (kg/m^2)	x	α_H (%)	α (%)	f (Hz)	ζ (%)	m (kg/m)	HEM model		VF model	
								$(m\delta/\rho_H D^2)$	V_p/fD	$(m\delta/\rho D^2)$	V_{eq}/fD
Present study: R–11, 40°C, $P/D = 1{\cdot}44$, $D = 0{\cdot}00635$ m, $f_a = 38{\cdot}8$ Hz, $\zeta_a = 0{\cdot}11\%$											
M01	478	0·0080	52·0	31·3	36·8	2·50	0·190	1·07	2·95	0·749	2·078
M02	425	0·0086	53·5	34·3	37·0	2·52	0·188	1·10	2·67	0·782	1·921
M03	396	0·0088	55·2	33·3	37·0	2·53	0·188	1·14	2·60	0·771	1·760
M04	389	0·0101	58·5	32·8	36·8	2·57	0·190	1·27	2·78	0·786	1·730
M05	356	0·0118	63·2	36·2	37·0	2·63	0·188	1·44	2·84	0·837	1·658
M06	308	0·0132	65·5	37·7	37·0	2·66	0·188	1·55	2·60	0·867	1·472
M07	296	0·0162	70·1	38·0	37·0	2·71	0·188	1·82	2·89	0·887	1·431
M08	250	0·0188	73·9	41·6	37·0	2·76	0·188	2·12	2·78	0·957	1·285
M09	205	0·0256	79·1	42·4	37·0	2·77	0·188	2·63	2·88	0·975	1·094
M10	176	0·0311	83·1	41·4	37·0	2·82	0·188	3·28	2·95	0·973	0·948
M11	130	0·0392	85·7	44·7	37·0	2·41	0·188	3·30	2·59	0·882	0·761
M12	98	0·0458	88·6	46·2	37·0	2·24	0·188	3·79	2·41	0·838	0·611
M13	86	0·0493	89·3	45·2	37·0	2·22	0·188	3·99	2·26	0·810	0·537
Pettigrew *et al.* (1989*b*): air–water, 22°C, $P/D = 1{\cdot}47$, $D = 0{\cdot}013$ m, $f_a = 33$ Hz, $\zeta_a = 0{\cdot}2\%$											
R-1	688	6·33e-5	5	2·9	26·7	1·1	0·50	0·22	2·09	0·211	2·05
R-2	688	2·12e-4	15	9·0	26·8	1·5	0·50	0·33	2·32	0·307	2·18
R-3	750	4·01e-4	25	15·8	27·0	2·0	0·49	0·49	2·85	0·434	2·54
R-4	775	8·02e-4	40	26·7	27·7	3·4	0·47	0·99	3·58	0·811	2·94
R-5	700	0·0012	50	33·8	28·3	3·9	0·45	1·30	3·80	0·987	2·88
R-6	689	0·0018	60	42·2	28·9	4·2	0·43	1·66	4·58	1·162	3·17
R-7	500	0·0036	75	54·1	29·5	3·4	0·41	2·08	5·20	1·126	2·84

R-9	320	0·0068	85	61·9	30·0	3·0	0·4	2·95	5·43	1·167	2·16
R-11	220	0·0107	90	65·9	30·2	3·0	0·39	4·35	5·54	1·267	1·66
R-13	160	0·0157	93	68·5	30·2	3·2	0·39	6·60	5·73	1·463	1·33
R-15	120	0·0224	95	70·6	30·4	3·1	0·39	8·77	5·94	1·518	1·09
R-17	100	0·0281	96	71·9	30·5	3·0	0·39	10·5	6·13	1·531	0·98
R-19	75	0·0375	97	72·7	30·4	2·9	0·39	13·5	6·09	1·525	0·81
R-21	55	0·0557	98	74·6	30·4	2·8	0·39	19·1	6·57	1·583	0·73
R-23	28	0·1060	99	76·0	30·5	2·9	0·39	37·3	6·31	1·736	0·57
Axisa *et al.* (1985): steam–water, 210°C, $P/D = 1{\cdot}44$, $D = 0{\cdot}019$ m, $f_a = 74$ Hz, $\zeta_a = 0{\cdot}2\%$											
A	1334	0·059	84·7	77·4	69·0	3·4	0·559	2·27	7·00	1·644	5·11
B	1111	0·090	89·7	82·8	69·8	2·3	0·546	2·15	8·27	1·406	5·48
C	709	0·117	92·1	84·4	70·0	1·8	0·540	2·11	6·67	1·197	3·90
D	518	0·186	95·3	88·3	72·1	1·6	0·532	2·85	7·28	1·364	3·76
E	392	0·250	96·7	90·2	71·0	1·3	0·529	3·04	7·39	1·293	3·57
F	306	0·340	97·8	92·2	71·8	1·0	0·526	3·13	7·68	1·204	3·60
Pettigrew *et al.* (1995): R-22, 23·3°C, $P/D = 1{\cdot}5$, $D = 0{\cdot}0127$ m, $f_a = 28{\cdot}5$ Hz, $\zeta_a = 0{\cdot}15\%$											
A	732	0·023	40	22·6	23·9	2·79	0·394	0·58	3·28	0·457	2·59
B	713	0·034	50	29·6	24·6	3·61	0·374	0·85	3·67	0·613	2·69
C	611	0·050	60	36·2	25·0	4·31	0·354	1·18	3·80	0·762	2·52
D	491	0·061	65	38·6	25·3	5·02	0·344	1·50	3·41	0·893	2·10
E	428	0·076	70	41·9	25·8	4·25	0·334	1·42	3·36	0·773	1·92
F	330	0·095	75	44·2	26·0	4·13	0·324	1·57	3·01	0·758	1·58
G	208	0·123	80	44·6	26·3	4·09	0·314	1·83	2·27	0·732	1·05
H	146	0·166	85	47·2	26·9	3·37	0·304	1·85	1·98	0·610	0·83
I	99	0·240	90	51·5	27·5	2·39	0·294	1·73	1·79	0·454	0·70

surface tension which is not scaled in the standard approach to tube bundle two-phase flow stability analysis. Indeed, the HEM approach considers that the only effect of two-phase flow is density variation and in the authors' opinion, does not even do that very well. Fluidelastic instability in two-phase flow is very complex and proper scaling should include such effects as surface tension, flow regime and velocity ratio (slip ratio) between the phases.

3.6.2. *Data comparison using void fraction modelling*

To the authors' knowledge, no attempt has previously been made to compare the existing fluidelastic instability data using a more accurate two-fluid model for determining the two-phase fluid parameters such as flow velocity and average density. Since it was established in Feenstra *et al.* (2000) that their new model is capable of predicting the void fraction in an upward two-phase flow in horizontal tube arrays for a variety of fluids, it is appropriate to recalculate the important parameters of the existing data and make such a comparison. The HEM void fraction, α_H, and predicted void fraction, α, are compared for each data set in Table 3. The average fluid density is determined using equation (2) except that the predicted void fraction, α, was utilized instead of the HEM void fraction, α_H. The equivalent flow velocity, V_{eq}, is determined from equation (7). The fluidelastic data of the other researchers were recalculated using the foregoing void fraction model and plotted on a stability diagram as shown in Figure 12(b), along with the data of the present study, in which the RAD void fraction was utilized. Note that the mass per unit length, m, and the vibration frequency, f, remained unchanged in the modified analysis. As was done in Figure 12(a), each data set is distinguished by the predicted flow regimes. By comparing the lower graph with the upper graph in Figure 12, it is clear that the new void fraction model has compressed each data set into a smaller range of mass-damping parameter. This is because the variation of average fluid density for each data set is smaller when analysed with the void fraction model as opposed to the HEM. The air–water data shows a remarkable change in behaviour between the predicted bubbly and intermittent flow regimes. In bubbly flow, the critical reduced velocity results follow a trend with mass-damping parameter which roughly agrees with Connors' formula as indicated by the solid line in both graphs of Figure 12. However, the data points corresponding to the intermittent flow regime show a significant reduction in critical reduced velocity over a small range of mass-damping parameter. Roughly, the same observation was made for the R-22 data, although in this case, some of the data points in the bubbly flow regime also show a decrease in stability with mass-damping parameter. The Axisa *et al.* steam–water data is rather tightly clustered in both graphs and it is difficult to observe any clear trends in stability behaviour, either with mass-damping parameter or flow regime. The R-11 data of the present study shows little variation in mass-damping parameter, yet it covers a significant range of reduced velocity.

3.6.3. *Comparison for other tube array geometries*

To extend the comparison, the fluidelastic instability data of the other researchers for other bundle array geometries, normal triangular, normal square (in-line) and rotated square were also analysed using both HEM and void fraction model analysis. The purpose of this extended analysis was to show that the flow regime effects observed for the parallel triangular tube array are also observed in the other array geometries and P/D ratios. The air–water results of Pettigrew *et al.* (1989*b*) for two normal triangular arrays of $P/D = 1{\cdot}47$ and $1{\cdot}32$, and a normal square array of $P/D = 1{\cdot}47$ are displayed in Figure 13(a,b). The upper graph presents the results analysed using the HEM. The data which corresponds to bubbly flow (open symbols) follows Connors' theory reasonably well, but

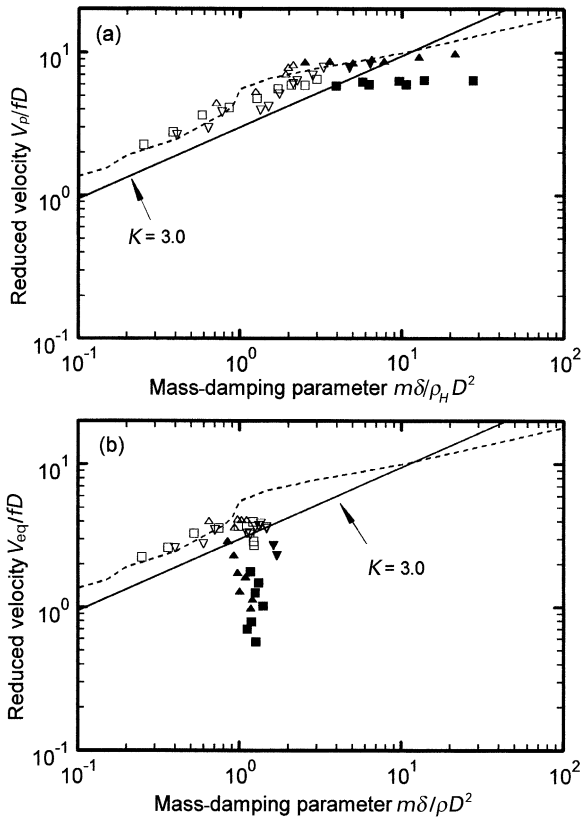

Figure 13. Critical flow velocities for fluidelastic instability for the data of Pettigrew *et al.* (1989*b*) for various tube arrays subjected to two-phase air–water cross-flow. Data analysis by (a) HEM model, and (b) void fraction model: □,■, normal square array, $P/D = 1.47$; ▽,▼, normal triangular array, $P/D = 1.32$; △,▲, normal triangular array, $P/D = 1.47$. ——, Connors' theory; - - -, prediction of Li & Weaver (1997). △,▽,□, Bubbly flow; ▲,▼,■, intermittent flow.

those data points which correspond to intermittent flow (solid symbols) deviate from this straight line relationship. In the lower graph, the same data are presented using the predictions of the void fraction model for determining average fluid density and equivalent flow velocity. In this case, it is clear that the same trends are observed in Figure 13(b) as in Figure 12(b), that the bubbly flow data remains in good agreement with the trend established by Connors' theory, but the data corresponding to intermittent flow departs significantly from this prediction. The application of the void fraction model has emphasized the downward turn of the intermittent flow data, so that the range of mass-damping parameter is reduced, while the values of the critical reduced velocity have changed from being relatively constant in the upper figure to decreasing significantly over a small range of mass-damping parameter in the lower figure.

The steam–water data of Axisa *et al.* (1985) and the R-12 data of Mann & Mayinger (1995) are presented in Figure 14, following the same comparison format as in the previous two figures. The data of Axisa *et al.* includes a normal triangular bundle and normal square bundle of $P/D = 1{\cdot}44$, but in this case the solid symbols correspond to the dispersed flow regime as predicted by Ulbrich & Mewes' map. The three data points of Mann & Mayinger (1995) are for a normal square bundle and correspond to bubbly flow only. In the upper graph, Figure 14(a), the data are analysed using the HEM while in the

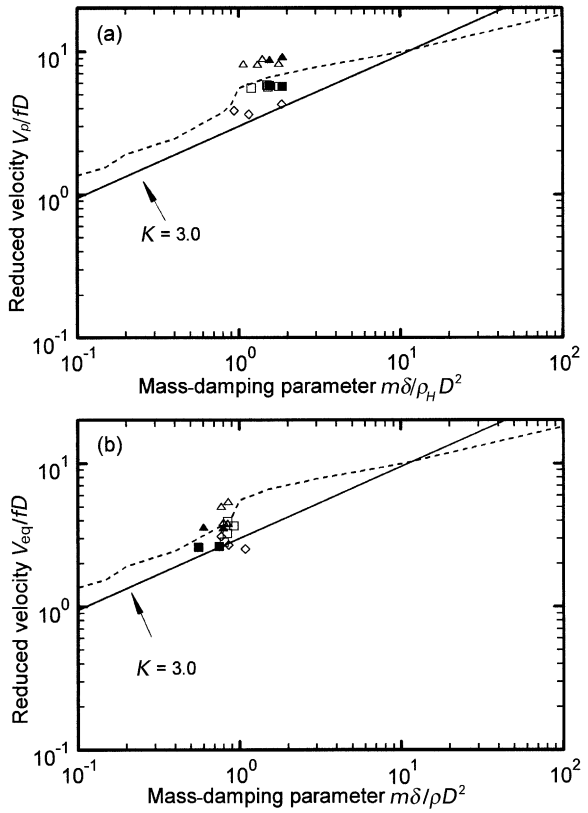

Figure 14. Critical flow velocities for fluidelastic instability for the data of other researchers for various tube arrays subjected to two-phase cross-flow. Data analysis by (a) HEM model, and (b) void fraction model: △, ▲, □, ■, Axisa *et al.* (1985) in steam–water; ◇, Mann & Mayinger (1995) in R-12. ———, Connors' theory; - - -, prediction of Li & Weaver (1997). △, □, ◇, Bubbly flow; ▲, ■, intermittent flow.

lower graph the data are analysed using the void fraction model. In this case, all of the data are clustered together and occupy only a small range of mass-damping parameter, which makes it difficult to discern any trends with respect to that parameter. However, it is clear that there exists no obvious difference between the bubbly flow data (open symbols) and the dispersed flow data (filled symbols). In the lower graph, Figure 14(b), the data is only slightly compressed in the horizontal direction, and the modified analysis indicates a slightly lower stability for the dispersed flow regime data versus the bubbly flow data. The data of Mann and Mayinger in the lower graph has slightly reversed in trend. In the upper graph, V_p/fD increased slightly with mass-damping parameter, while in the lower graph this trend is opposite. However, a significant decrease in stability is not observed, which is consistent with behaviour of the bubbly flow data in the previous two figures.

Returning to Figs. 12(b) and 13(b), it was shown that the application of the void fraction model resulted in a significant departure from the predicted stability behaviour for the data points corresponding to the intermittent flow regime. It is observed that each set of these data points (filled symbols) correspond to nearly the same mass-damping parameter, and yet they cover nearly a decade of critical reduced velocity values. In each case, the lowest values of V_{eq}/fD correspond to flows with the highest void fraction. Such a trend creates uncertainty for the designer who wishes to predict the stability limit of a particular heat exchanger design, since it is normally expected that the critical reduced

velocity should have a single-valued relationship with mass-damping parameter. The analysis suggests that reduced velocity and mass-damping parameters alone may be insufficient to properly model flow-induced vibration in the intermittent flow regime of two-phase flows, and that there are added complications in this type of two-phase flow which the present analysis neglects. One possible factor is the ratio of bubble size to tube diameter, which could affect the pressure drop of the flow through the array and the fluid damping. It may also play a role in the level and correlation length of turbulent forces on the tubes in the array. The present authors have observed that the average bubble size increases with void fraction and decreases slightly with mass flux. At very low void fractions (below 10%) the vapour bubbles are small, have roughly the same velocity and are distributed fairly evenly across the cross-section of the flow conduit. As void fraction rises, however, the average bubble size increases and the large bubbles travel upward faster, while the smaller bubbles travel slower and often stagnate or become entrained in the periodic liquid down-wash. When the void fraction increases further to the point where the flow regime becomes intermittent, the flow is no longer steady, and periodic upward surges of high void fraction flow occurs, followed by periods of bubble stagnation and liquid down-wash. In such a case, defining an average or equivalent flow velocity for fluidelastic threshold calculations may be inappropriate. Additionally, a nonlinear softening effect may be occurring, whereby the flow surges may be sufficient to trigger the instability in a nonadjacent equilibrium state. Since the fluidelastic forces are self-excited, the high amplitude vibrations brought on by such transient events may persist even if the flow velocity reduces below the critical velocity but not into the subcritical range. Since the intermittent flow regime is characterized by substantial fluctuations in flow velocity and void distribution, it has the potential for initiating fluidelastic instability at flow rates lower than normally expected for steady flow. The fact that the stability threshold decreases for lower mass flux levels (corresponding to higher void fractions) is consistent with the fact that the intermittency is more pronounced at higher void fractions, so long as dispersed flow is not approached. However, more research is necessary to rigorously establish a velocity criterion for fluidelastic instability in two-phase flow, especially in the intermittent flow regime.

4. CONCLUSIONS

The modelling process for studying flow-induced vibration of a parallel triangular tube array subjected to two-phase R-11 flow has been presented along with a comparison of the stability behaviour of this array with data of other researchers. The primary intent of the research was to explore a new method of stability analysis which incorporates more realistic modelling of the two-phase flow.

The experimental results of the present study showed that the actual void fraction obtained with the radiation attenuation detection method (RAD) was significantly less than that assumed by the homogeneous equilibrium model (HEM). This difference arises because the HEM neglects velocity differences between the phases and has important implications for the accurate determination of two-phase fluid parameters such as average density and equivalent flow velocity. A relatively simple model for determining improved void fraction predictions has been developed and is used for data analysis in this paper.

Damping measurements were obtained from the single flexible tube array, showing that the tube damping in two-phase cross-flow peaks at about 75 to 80% HEM void fraction. This is in qualitative agreement with air–water and R-22 data from the literature. Comparison has revealed that, while the measured two-phase damping values in R-11 are

slightly lower than comparable air–water data, the normalized two-phase component of damping is actually a bit higher than in air–water, owing to the large difference in liquid mass ratio (a normalizing parameter) between these two sets of data. However, it must be noted that the present normalizing parameters are still in the developmental stages, since the effects of liquid surface tension or flow regime have not been adequately determined.

The use of the improved void fraction model for analysing fluidelastic instability data has shown some interesting results. The improved estimate for average fluid density has significantly reduced that range of the mass-damping parameter for the various modelling fluids. At the same time, it has greatly enhanced the change in stability trend associated with a change in flow regime from bubbly to intermittent flow, and the data collapse in the latter flow regime has been substantially improved. The analysis presented in this paper is considered to be only a step in the direction of improved modelling for fluidelastic instability of tube bundles in two-phase flow. More research is needed in order to better account for the effects of surface tension, bubble or liquid droplet size and distribution, and flow regime.

ACKNOWLEDGEMENTS

The authors are grateful for the financial support of the Natural Science and Engineering Research Council of Canada and Atomic Energy of Canada Limited through a Cooperative Research and Development Grant.

REFERENCES

Axisa, F., Boheas, M. A. & Villard, B. 1985 Vibration of tube bundles subjected to steam–water cross-flow: a comparative study of square and triangular arrays. *Paper B*1/2 in the *8th International Conference on Structural Mechanics in Reactor Technology,* Brussels Belgium.

Chan, A. M. C. & Bannerjee, S. 1981 Design aspects of gamma densitometers for void fraction measurements in small scale two-phase flows. *Nuclear Instruments and Methods* **190,** 135–148.

Chen, S. S. 1983 Instability mechanisms and stability criteria of a group of circular cylinders subjected to cross-flow, Part I: theory; Part II: numerical results and discussions. *ASME Journal of Vibration, Acoustics, Stress and Reliability in Design* **105,** 51–58 and 235–260.

Dowlati, R., Kawaji, M. D., Chisholm, D. & Chan, A. M. C. 1992 Void fraction prediction in two-phase flow across a tube bundle. *AIChE Journal* **38,** 619–622.

Feenstra, P. A. 2000 Modelling two-phase flow-excited fluidelastic instability in heat exchanger tube arrays. Ph.D. thesis, Department of Mechanical Engineering, McMaster University, Hamilton, Canada.

Feenstra, P. A., Judd, R. L. & Weaver, D. S. 1995 Fluidelastic instability in a tube array subjected to two-phase R-11 cross-flow. *Journal of Fluids and Structures* **9,** 747–771.

Feenstra, P. A., Weaver, D. S. & Judd, R. L. 2000 An improved void fraction model for two-phase cross-flow through horizontal tube arrays. *International Journal of Multiphase Flow* **26,** 1851–1873.

Grant, I. D. R. & Murray, I. 1972 Pressure drop on the shell-side of a segmentally baffled shell-and-tube heat exchanger with vertical two-phase flow. *Report NEL-560*. National Engineering Laboratory, Glasgow, Scotland.

Harris, R. E., Dokainish, M. A. & Weaver, D. S. 1985 A simplified finite element for added mass and inertial coupling in arrays of cylinders. *ASME Journal of Pressure Vessel Technology* **107,** 118–125.

Judd, R. L., Dam, R. & Weaver, D. S. 1992 A photo-optical technique for measuring flow-induced vibrations in cantilevered tube bundles. *Experimental Thermal and Fluid Science* **5,** 747–754.

Li, M. & Weaver, D. S. 1997 An fluidelastic instability model with an extension to full flexible multi-span tube arrays. In *Proceedings of the ASME PVP Conference* (*Dallas*), Vol. II. *Flow-Induced Vibration and Noise*.

LEVER, J. H. & WEAVER, D. S. 1986 On the stability of heat exchanger tube bundles, Part II: numerical results and comparison with experiments. *Journal of Sound and Vibration* **107,** 393–410.

MANN, W. & MAYINGER, F. 1995 Flow-induced vibration of tube bundles subjected to single and two-phase cross-flow. *Proceedings 2nd International Conference on Multiphase Flow*, Vol. 4, pp. 9–15, Kyoto, Japan.

MCADAMS, W. H., WOODS, W. K. & HEROMAN, L. C. 1942 Vapourization inside horizontal tubes–II. Benzene–oil mixtures. *Transactions of the ASME* **64,** 193–200.

PAÏDOUSSIS, M. P. 1982 A review of flow-induced vibrations in reactors and reactor components. *Nuclear Engineering & Design* **74,** 31–60.

PETTIGREW, M. J. & KNOWLES, G. D. 1997 Some aspects of heat exchanger tube damping in two-phase mixtures. *Journal of Fluids and Structures* **11,** 929–945.

PETTIGREW, M. J., ROGERS, R. J. & AXISA, F. 1986 Damping of multispan heat exchanger tubes—Part 2: in liquids. In *Flow-Induced Vibration—1986*, PVP-Vol. 104 (eds S. S. CHEN, J. C. SIMONIS & Y. S. SHIN), pp. 89–98. New York: ASME.

PETTIGREW M. J. & TAYLOR, C. E. 1994 Two-phase flow-induced vibration: an overview. *ASME Journal of Pressure Vessel Technology* **116,** 233–253.

PETTIGREW, M. J., TAYLOR, C. E. JONG, J. H. & CURRIE, I. G.1995 Vibration of a tube bundle in two-phase freon cross-flow. *ASME Journal of Pressure Vessel Technology* **117,** 321–329.

PETTIGREW, M. J., TAYLOR, C. E. & KIM, B. S. 1989*a* Vibration of tube bundles in two-phase cross flow. Part 1—hydrodynamic mass and damping. *ASME Journal of Pressure Vessel Technology* **111,** 466–477.

PETTIGREW, M. J., TROMP, J. H., TAYLOR, C. E. & KIM, B. S. 1989*b* Vibration of tube bundles in two-phase cross-flow. Part 2—fluid-elastic instability. *ASME Journal of Pressure Vessel Technology* **111,** 478–487.

ROGERS, R. G., TAYLOR, C. E. & PETTIGREW, M. J. 1984 Fluid effects on multi-span heat exchanger tube vibration. *ASME PVP Conference*, San Antonio, TX, U.S.A. pp. 17–26.

SCHRAGE, D. S., HSU, J.-T. & JENSEN, M. K. 1988 Two-phase pressure drop in vertical cross-flow across a horizontal tube bundle. *AIChE Journal* **34,** 107–115.

TAITEL, Y., BORNEA, D. & DUKLER, A. E. 1980 Modelling flow pattern transitions for steady, upward gas-liquid flow in vertical tubes. *AIChE Journal* **26,** 345–354.

ULBRICH, R. & MEWES, D. 1994 Vertical, upward gas-liquid two-phase flow across a tube bundle. *International Journal of Multiphase Flow* **20,** 249–272.

WEAVER, D. S. & FITZPATRICK, J. A. 1988 A review of cross-flow induced vibrations in heat exchanger tube arrays. *Journal of Fluids and Structures* **2,** 73–93.

WEAVER, D. S. & KOROYANNAKIS, D. 1982 The cross-flow response of a tube array in water—A comparison with the same array in air. *ASME Journal of Pressure Vessel Technology* **104,** 139–146.

ZUBER, N. & FINDLAY, J. A. 1965 Average volumetric concentration in two-phase flow systems. *ASME Journal of Heat Transfer* **87,** 453–468.

APPENDIX: NOMENCLATURE

A	cross-sectional area, m^2
Cap	Capillary number
D	tube diameter, m
D/D_e	tube confinement ratio
f	frequency of vibration, Hz
g	gravitational acceleration, m/s^2
G	mass flux, $kg/m^2\,s$
K	Connors' constant
m	tube mass per unit length including added fluid mass, kg/m
m_t	tube mass per unit length, kg/m
m_R	added mass ratio
N	gamma count in two-phase fluid medium
N_G	gamma count in gas-phase medium

N_L	gamma count in liquid-phase medium
Ri	Richardson number
S	slip ratio
U_G	gas phase velocity, m/s
U_L	liquid phase velocity, m/s
U_{Gs}	superficial gas phase velocity, m/s
U_{Ls}	superficial liquid phase velocity, m/s
V_p	pitch flow velocity, m/s
x	flow quality
Greek letters	
α	void fraction
$\Delta\rho$	density difference between phases, kg/m^3
δ	logarithmic decrement damping
ζ	damping ratio
μ	absolute viscosity, Pa s
v	relative viscosity, m^2/s
ρ	fluid density, kg/m^3
σ	liquid surface tension, N/m
Subscripts	
a	quantity measured in air
eq	equivalent quantity
Crit	critical value at the fluidelastic threshold
G	gas phase
Gs	superficial gas phase
H	quantity calculated by the homogeneous equilibrium model
L	liquid phase
Ls	superficial liquid phase
p	pitch quantity
s	structural component
TP	two-phase component
u	upstream quantity
V	viscous component
pred	predicted value
RAD	quantity corresponding to radiation attenuation detection method of void fraction measurement
HEM	quantity corresponding to homogeneous equilibrium model for void fraction measurement